Spatio-angular transfer functions for polarized fluorescence microscopes

Talon Chandler, Min Guo, Hari Shroff, Rudolf Oldenbourg, Patrick La Rivière

April 30, 2018

1 Introduction

These notes are a continuation of the 2018-02-23 notes on the spatio-angular transfer functions for unpolarized fluorescence microscopes. We will use the same notation and extend those results to microscopes with polarized illumination and detection.

2 Polarized illumination

We can model polarized excitation using a spatio-angular excitation point response function $h_{\text{exc}}(\mathbf{r}_o, \hat{\mathbf{s}}_o)$. In these notes we will only consider spatially uniform excitation patterns $h_{\text{exc}}(\hat{\mathbf{s}}_o)$, but we would need the full function to model structured illumination patterns.

We calculated several spatio-angular excitation point response functions in our Optics Express paper [1] (in the paper we called this function the excitation efficiency for a single dipole, but this is equivalent to the excitation point spread function). If we place a spatially incoherent and spatially uniform light source (or its image) in the aperture plane with the optical axis along the $\hat{\mathbf{z}}$ axis, then the excitation point response function is given by

$$h_{\text{exc}}^{\hat{\mathbf{z}}}(\Theta, \Phi; \phi_{\text{exc}}) = \bar{D}\{\bar{A} + \bar{B}\sin^2\Theta + \bar{C}\sin^2\Theta\cos\left[2(\Phi - \phi_{\text{exc}})\right]\}, \tag{1}$$

where $\hat{\mathbf{s}}_o = \cos\Phi\sin\Theta\hat{\mathbf{x}} + \sin\Phi\sin\Theta\hat{\mathbf{y}} + \cos\Theta\hat{\mathbf{z}}$, the illumination polarizer orientation is given by $\hat{\mathbf{p}} = \cos\phi_{\text{exc}}\hat{\mathbf{x}} + \sin\phi_{\text{exc}}\hat{\mathbf{y}}$, and

$$\bar{A} = \frac{1}{4} - \frac{3}{8}\cos\alpha + \frac{1}{8}\cos^3\alpha, \tag{2a}$$

$$\bar{B} = \frac{3}{16}\cos\alpha - \frac{3}{16}\cos^3\alpha, \tag{2b}$$

$$\bar{C} = \frac{7}{32} - \frac{3}{32}\cos\alpha - \frac{3}{32}\cos^2\alpha - \frac{1}{32}\cos^3\alpha, \tag{2c}$$

$$\bar{D} = \frac{4}{3(1-\cos\alpha)}, \tag{2d}$$

where $\alpha = \arcsin(\text{NA}/n_o)$. I'm using bars on the constants to avoid notation overlap with the previous note set. We can rewrite this expression in terms of spherical harmonics as

$$\begin{aligned} h_{\text{exc}}^{\hat{\mathbf{z}}}(\hat{\mathbf{s}}_o; \hat{\mathbf{p}}) \propto\ & [2\bar{A} + (4/3)\bar{B}]y_0^0(\hat{\mathbf{s}}_o) - \frac{4\sqrt{5}}{15}\bar{B}y_2^0(\hat{\mathbf{s}}_o) + \\ & \frac{4\bar{C}}{\sqrt{15}}\left\{[(\hat{\mathbf{p}}\cdot\hat{\mathbf{x}})^2 - (\hat{\mathbf{p}}\cdot\hat{\mathbf{y}})^2]y_2^2(\hat{\mathbf{s}}_o) - 2(\hat{\mathbf{p}}\cdot\hat{\mathbf{x}})(\hat{\mathbf{p}}\cdot\hat{\mathbf{y}})y_2^{-2}(\hat{\mathbf{s}}_o)\right\}. \end{aligned} \tag{3}$$

The light-sheet excitation point response function is given by Eq. 3 in the limit of small NA which gives

$$h_{\text{exc}}^{\hat{\mathbf{z}},\text{ls}}(\hat{\mathbf{s}}_o; \hat{\mathbf{p}}) \equiv \lim_{\alpha\to 0} h_{\text{exc}}^{\hat{\mathbf{z}}}(\hat{\mathbf{s}}_o) \propto y_0^0(\hat{\mathbf{s}}_o) + \frac{7}{4\sqrt{15}}\left\{[(\hat{\mathbf{p}}\cdot\hat{\mathbf{x}})^2 - (\hat{\mathbf{p}}\cdot\hat{\mathbf{y}})^2]y_2^2(\hat{\mathbf{s}}_o) - 2(\hat{\mathbf{p}}\cdot\hat{\mathbf{x}})(\hat{\mathbf{p}}\cdot\hat{\mathbf{y}})y_2^{-2}(\hat{\mathbf{s}}_o)\right\}. \tag{4}$$

To find the excitation point response function for illumination along the $\hat{\mathbf{x}}$ axis we need to change every $\hat{\mathbf{x}}$ and $\hat{\mathbf{y}}$ to $\hat{\mathbf{z}}$ and $-\hat{\mathbf{y}}$, respectively. Rotating the spherical harmonics is not trivial, but we show the relevant

transformation matrix in Appendix A. The excitation point response function for illumination along the $\hat{\mathbf{x}}$ axis is given by

$$h_{\text{exc}}^{\hat{\mathbf{x}},\text{ls}}(\hat{\mathbf{s}}_o;\hat{\mathbf{p}}) \propto y_0^0(\hat{\mathbf{s}}_o) + \frac{7}{4\sqrt{15}}\left\{[(\hat{\mathbf{p}}\cdot\hat{\mathbf{z}})^2 - (\hat{\mathbf{p}}\cdot\hat{\mathbf{y}})^2]\left[\frac{\sqrt{3}}{2}y_2^0(\hat{\mathbf{s}}_o) + \frac{1}{2}y_2^2(\hat{\mathbf{s}}_o)\right] + 2(\hat{\mathbf{p}}\cdot\hat{\mathbf{z}})(\hat{\mathbf{p}}\cdot\hat{\mathbf{y}})y_2^{-1}(\hat{\mathbf{s}}_o)\right\}. \quad (5)$$

To find the excitation transfer functions we need to calculate

$$H_{l,\text{exc}}^m = \int_{\mathbb{S}^2} d\hat{\mathbf{s}}_o\, h_{\text{exc}}(\hat{\mathbf{s}}_o) y_l^m(\hat{\mathbf{s}}_o). \quad (6)$$

This calculation is straightforward now that we've expressed the excitation point response functions in terms of spherical harmonics. The excitation transfer functions are

$$H_{l,\text{exc}}^{m,\hat{\mathbf{z}}}(\hat{\mathbf{p}}) \propto [2\bar{A} + (4/3)\bar{B}]\delta(l,m) - \frac{4\sqrt{5}}{15}\bar{B}\delta(l-2,m)(\hat{\mathbf{s}}_o) + \frac{4\bar{C}}{\sqrt{15}}\left\{[(\hat{\mathbf{p}}\cdot\hat{\mathbf{x}})^2 - (\hat{\mathbf{p}}\cdot\hat{\mathbf{y}})^2]\delta(l-2,m-2) - 2(\hat{\mathbf{p}}\cdot\hat{\mathbf{x}})(\hat{\mathbf{p}}\cdot\hat{\mathbf{y}})\delta(l-2,m+2)\right\}, \quad (7)$$

$$H_{l,\text{exc}}^{m,\hat{\mathbf{z}},\text{ls}}(\hat{\mathbf{p}}) \propto \delta(l,m) + \frac{7}{4\sqrt{15}}\left\{[(\hat{\mathbf{p}}\cdot\hat{\mathbf{x}})^2 - (\hat{\mathbf{p}}\cdot\hat{\mathbf{y}})^2]\delta(l-2,m-2) - 2(\hat{\mathbf{p}}\cdot\hat{\mathbf{x}})(\hat{\mathbf{p}}\cdot\hat{\mathbf{y}})\delta(l-2,m+2)\right\}, \quad (8)$$

$$H_{l,\text{exc}}^{m,\hat{\mathbf{x}},\text{ls}}(\hat{\mathbf{p}}) \propto \delta(l,m) + \frac{7}{4\sqrt{15}}\left\{[(\hat{\mathbf{p}}\cdot\hat{\mathbf{z}})^2 - (\hat{\mathbf{p}}\cdot\hat{\mathbf{y}})^2]\left[\frac{\sqrt{3}}{2}\delta(l-2,m) + \frac{1}{2}\delta(l-2,m-2)\right] + 2(\hat{\mathbf{p}}\cdot\hat{\mathbf{z}})(\hat{\mathbf{p}}\cdot\hat{\mathbf{y}})\delta(l-2,m+1)\right\}. \quad (9)$$

3 Polarized detection

In the previous note set we found the spatio-angular detection point spread function for unpolarized fluorescence microscopes. In this section we will find the spatio-angular detection point spread function when there is a linear polarizer in the detection path.

The electric field in the back-focal plane of a fluorescence microscope under the paraxial approximation is given by

$$\tilde{\mathbf{e}}_b^{(p)}(\mathbf{r}_b;\mathbf{r}_o,\hat{\mathbf{s}}_o) \propto \begin{bmatrix} y_1^1(\hat{\mathbf{s}}_o) - \frac{2r_b}{f_o}\cos\phi_b y_1^0(\hat{\mathbf{s}}_o) \\ y_1^{-1}(\hat{\mathbf{s}}_o) - \frac{2r_b}{f_o}\sin\phi_b y_1^0(\hat{\mathbf{s}}_o) \\ 0 \end{bmatrix}. \quad (10)$$

In these notes we will ignore the phase term in the back focal plane—see the previous notes for more details on shift invariance. Alternatively, we can say that Eq. 10 is the electric field in the back focal plane created by a single dipole at the focal point of the objective.

If we place a polarizer oriented along $\hat{\mathbf{p}}_d$ in the back focal plane then the electric field becomes

$$\tilde{\mathbf{e}}_b^{(p)}(\mathbf{r}_b;\mathbf{r}_o,\hat{\mathbf{s}}_o) \propto \hat{\mathbf{p}}_d \cdot \begin{bmatrix} y_1^1(\hat{\mathbf{s}}_o) - \frac{2r_b}{f_o}\cos\phi_b y_1^0(\hat{\mathbf{s}}_o) \\ y_1^{-1}(\hat{\mathbf{s}}_o) - \frac{2r_b}{f_o}\sin\phi_b y_1^0(\hat{\mathbf{s}}_o) \\ 0 \end{bmatrix}. \quad (11)$$

To find the electric field in the detector plane we need to take the two-dimensional Fourier transform of each component. The dot product with the polarizer is linear, so we can pull the Fourier transform inside and use the same result from the previous notes

$$\tilde{\mathbf{e}}_d'^{(p)}(\mathbf{r}_o',\hat{\mathbf{s}}_o;\hat{\mathbf{p}}_d) \propto \hat{\mathbf{p}}_d \cdot \begin{bmatrix} a^{(p)}(r_o')y_1^1(\hat{\mathbf{s}}_o) + 2ib^{(p)}(r_o')\cos\phi_o' y_1^0(\hat{\mathbf{s}}_o) \\ a^{(p)}(r_o')y_1^{-1}(\hat{\mathbf{s}}_o) + 2ib^{(p)}(r_o')\sin\phi_o' y_1^0(\hat{\mathbf{s}}_o) \\ 0 \end{bmatrix}. \quad (12)$$

Finally, we can find the spatio-angular point spread function by taking the squared modulus of the electric field on the detector

$$h'^{(p)}(\mathbf{r}'_o, \hat{\mathbf{s}}_o; \hat{\mathbf{p}}_d) \equiv |\tilde{\mathbf{e}}'^{(p)}_d(\mathbf{r}'_o, \hat{\mathbf{s}}_o; \hat{\mathbf{p}}_d)|^2. \tag{13}$$

Expanding, factoring, and normalizing the result gives

$$h'^{(p)}(\mathbf{r}'_o, \hat{\mathbf{s}}_o; \hat{\mathbf{p}}_d) = h'^{0(p)}_0(\mathbf{r}'_o) y^0_0(\hat{\mathbf{s}}_o) + h'^{0(p)}_2(\mathbf{r}'_o) y^0_2(\hat{\mathbf{s}}_o) + h'^{2(p)}_2(\mathbf{r}'_o) y^2_2(\hat{\mathbf{s}}_o) + h'^{-2(p)}_2(\mathbf{r}'_o) y^{-2}_2(\hat{\mathbf{s}}_o), \tag{14}$$

where

$$h'^{0(p)}_0(\mathbf{r}'_o; \hat{\mathbf{p}}_d) \equiv a^{(p)2}(r'_o) + 4b^{(p)2}(r'_o)(\hat{\mathbf{r}}'_o \cdot \hat{\mathbf{p}}_d)^2, \tag{15}$$

$$h'^{0(p)}_2(\mathbf{r}'_o; \hat{\mathbf{p}}_d) \equiv \frac{1}{\sqrt{5}} \left[-a^{(p)2}(r'_o) + 8b^{(p)2}(r'_o)(\hat{\mathbf{r}}'_o \cdot \hat{\mathbf{p}}_d)^2 \right], \tag{16}$$

$$h'^{2(p)}_2(\mathbf{r}'_o; \hat{\mathbf{p}}_d) \equiv \sqrt{\frac{3}{5}} a^{(p)2}(r'_o) \left[(\hat{\mathbf{p}}_d \cdot \hat{\mathbf{x}})^2 - (\hat{\mathbf{p}}_d \cdot \hat{\mathbf{y}})^2 \right], \tag{17}$$

$$h'^{-2(p)}_2(\mathbf{r}'_o; \hat{\mathbf{p}}_d) \equiv -2\sqrt{\frac{3}{5}} a^{(p)2}(r'_o)(\hat{\mathbf{p}}_d \cdot \hat{\mathbf{x}})(\hat{\mathbf{p}}_d \cdot \hat{\mathbf{y}}). \tag{18}$$

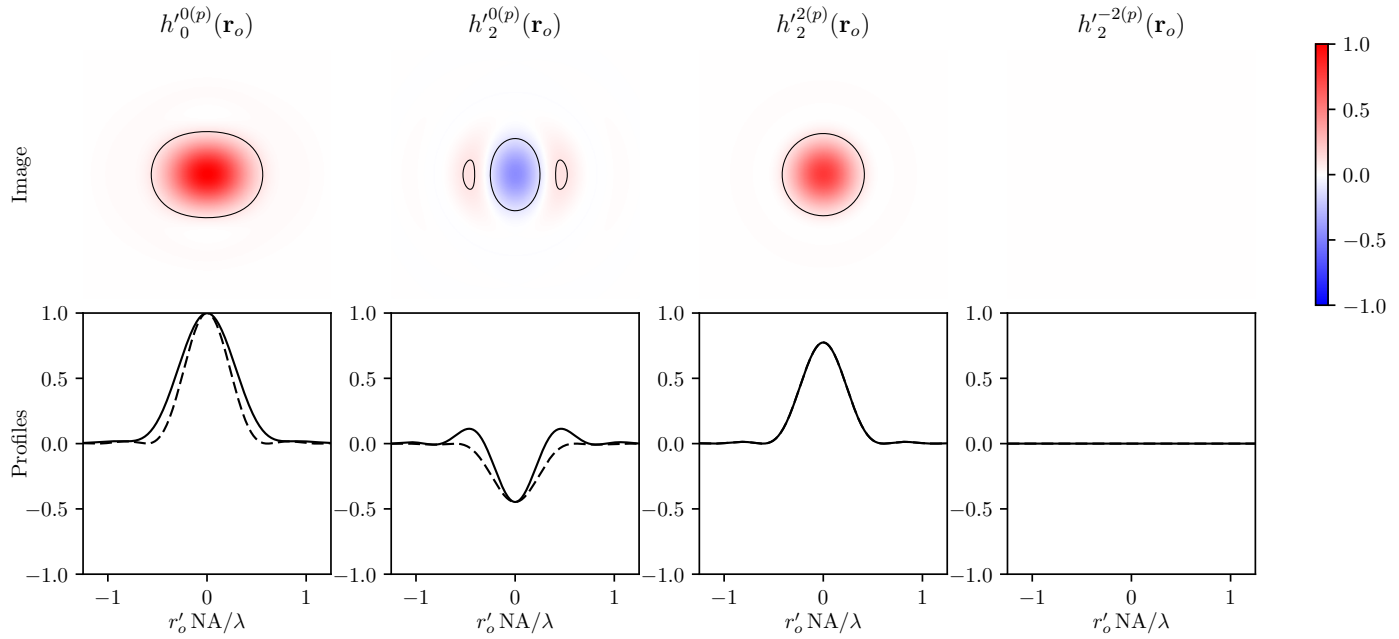

Figure 1: Spatio-angular point spread function for a single-view fluorescence microscope with NA = 0.8, $n_o = 1.33$ and an $\hat{\mathbf{x}}$-oriented polarizer under the paraxial approximation. **Columns:** Each term of the spatio-angular point spread function. **Row 1:** Images of each term with contours at ± 0.1 and **Row 2:** horizontal (solid) and vertical (dashed) profiles through each term. The h'^0_0 and h'^0_2 terms have a $\cos^2\phi_o$ dependence, so two profiles are sufficient to characterize their images. The h'^2_2 and h'^{-2}_2 terms are radially symmetric, so one profile is sufficient.

The spatio-angular point spread function for a fluorescence microscope with a polarized detection path has four terms—see Figures 1 and 2 for plots. The h'^0_0 and h'^2_0 terms are familiar from the unpolarized case, but now they have an extra factor of $(\mathbf{r}'_o \cdot \hat{\mathbf{p}}_d)^2$ that accounts for the polarizer and breaks radial symmetry. Notice that if we average over all polarizer orientations then $(\mathbf{r}'_o \cdot \hat{\mathbf{p}}_d)^2 \to 1/2$, and we recover the spatio-angular point spread function for a microscope without a detection polarizer.

One of the interesting predictions of the polarized spatio-angular point spread function is the elongated point spread function in the $h_0'^0$ term (which corresponds to a physically realizable uniform distribution of dipoles). The long axis of the point spread function is parallel with the transmission axis of the polarizing filter—this is not an intuitive result. If we applied the usual reasoning for the width of point spread functions—broader distributions of intensity in the back focal plane cause narrower point spread functions—we would predict that the point spread function for the $h_0'^0$ term would be elongated perpendicular to the transmission axis of the polarizer. This reasoning fails because we need to add the intensities at the detector, not at the back focal plane.

The $h_2'^2$ and $h_2'^{-2}$ terms are only non-zero when a polarizing filter is in the detection path. These terms correspond to distributions of fluorophores with positive and negative fluorophores near the transverse plane only. Without a polarizer, the "intensity contributions" from the positive and negative fluorophores cancel, and we have no contribution from these distributions. With a polarizer, the intensity contribution from the positive or negative fluorophores dominate, and we end up with a rotationally symmetric contribution to the point spread function.

It's interesting to compare polarizing filters with phase and amplitude filters. Adding a phase filter can extend the band limit of a microscope to measure new information about the object without blocking any photons. For example, cubic phase masks and microlens arrays can increase the axial band limit of a microscope. All lenses can be considered as phase filters, so it's almost obvious that phase filters can increase the band limit of an imaging system. Amplitude filters, on the other hand, cannot extend the band limit of a microscope. Amplitude filters can change the contrast for different spatial frequencies by blocking photons, but they do not allow new information to be measured. Polarizing filters share properties with phase and amplitude filters—they block photons **and** extend the angular band limit of the microscope.

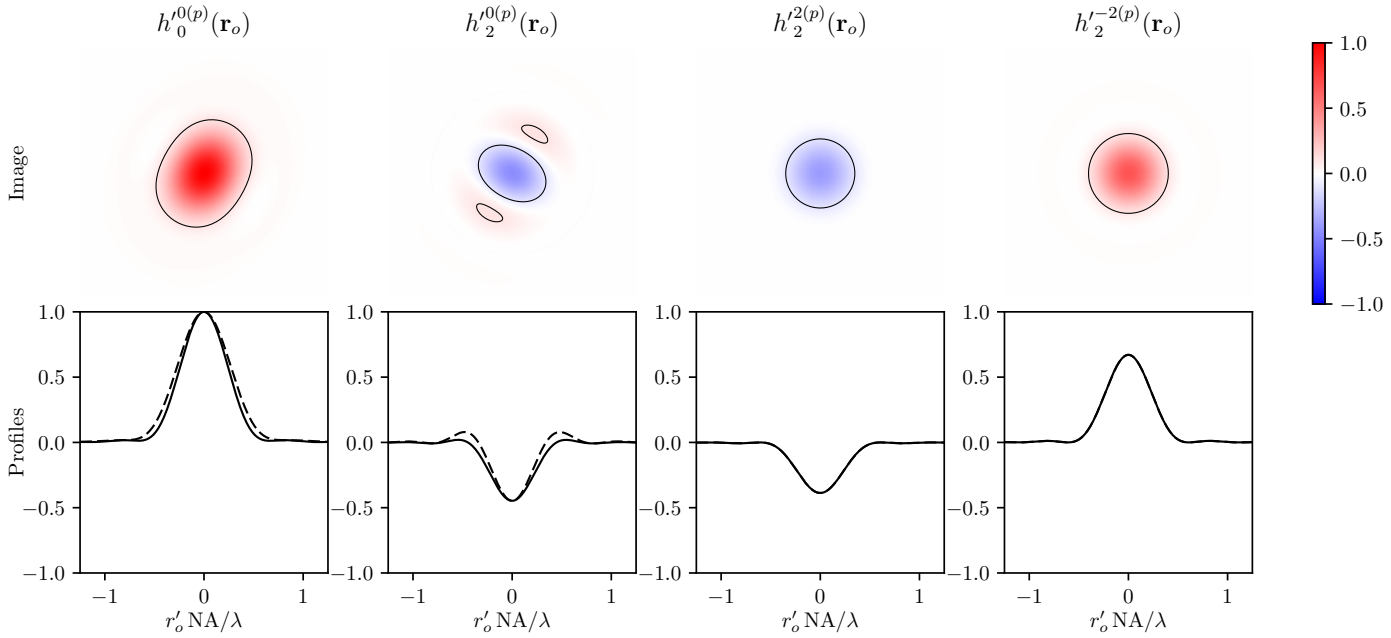

Figure 2: Spatio-angular point spread function for a single-view fluorescence microscope with NA = 0.8, $n_o = 1.33$ and an $(\hat{\mathbf{x}}/2 + \sqrt{3}\hat{\mathbf{y}}/2)$-oriented polarizer under the paraxial approximation. **Columns:** Each term of the spatio-angular point spread function. **Row 1:** Images of each term with contours at ± 0.1 and **Row 2:** horizontal (solid) and vertical (dashed) profiles through each term. The $h_0'^0$ and $h_2'^0$ terms have a $\cos^2 \phi_o$ dependence, so two profiles are sufficient to characterize their images. The $h_2'^2$ and $h_2'^{-2}$ terms are radially symmetric, so one profile is sufficient.

To find the transfer function we need to calculate the Fourier transform of the point spread function. We can use the following Fourier transforms that we evaluated in the previous notes

$$\mathcal{F}_2\left\{{a^{(p)}}^2(r_o')\right\} = 8\left[\arccos\left(\frac{\nu}{2\nu_o}\right) - \frac{\nu}{2\nu_o}\sqrt{1-\left(\frac{\nu}{2\nu_o}\right)^2}\right]\Pi\left(\frac{\nu}{2\nu_o}\right), \tag{19}$$

$$\mathcal{F}_2\left\{{b^{(p)}}^2(r_o')\cos^2\phi_o'\right\} = 4\left(\frac{\mathrm{NA}}{n_o}\right)^2\left[\arccos\left(\frac{\nu}{2\nu_o}\right) - \frac{1}{3}\left[5-2\left(\frac{\nu}{2\nu_o}\right)^2\right]\frac{\nu}{2\nu_o}\sqrt{1-\left(\frac{\nu}{2\nu_o}\right)^2} - \frac{8}{3}\cos^2\phi_\nu\frac{\nu}{2\nu_o}\sqrt[3]{1-\left(\frac{\nu}{2\nu_o}\right)}\right]\Pi\left(\frac{\nu}{2\nu_o}\right). \tag{20}$$

Applying these results and normalizing gives the spatio-angular transfer function for a fluorescence microscope with a polarizer along the detection path

$$H_m^{l(p)}(\boldsymbol{\nu};\hat{\mathbf{p}}_d) = H_0^{0(p)}(\boldsymbol{\nu})\delta(l,m) + H_2^{0(p)}(\boldsymbol{\nu})\delta(l-2,m) + H_2^{2(p)}(\nu)\delta(l-2,m-2) + H_2^{-2(p)}(\nu)\delta(l-2,m+2), \tag{21}$$

where

$$H_0^{0(p)}(\boldsymbol{\nu};\hat{\mathbf{p}}_d) \equiv \frac{1}{1+(\mathrm{NA}/n_o)^2}\left[A^{(p)}(\nu) + 2B^{(p)}(\nu) + 2C^{(p)}(\nu)\left\{2(\hat{\boldsymbol{\nu}}\cdot\hat{\mathbf{p}}_d)^2-1\right\}\right], \tag{22}$$

$$H_2^{0(p)}(\boldsymbol{\nu};\hat{\mathbf{p}}_d) \equiv \frac{1}{\sqrt{5}[1+(\mathrm{NA}/n_o)^2]}\left[-A^{(p)}(\nu) + 4B^{(p)}(\nu) + 4C^{(p)}(\nu)\left\{2(\hat{\boldsymbol{\nu}}\cdot\hat{\mathbf{p}}_d)^2-1\right\}\right], \tag{23}$$

$$H_2^{2(p)}(\nu;\hat{\mathbf{p}}_d) \equiv \sqrt{\frac{3}{5}}\frac{1}{[1+(\mathrm{NA}/n_o)^2]}A^{(p)}(\nu)\left[(\hat{\boldsymbol{\nu}}\cdot\hat{\mathbf{x}})^2 - (\hat{\boldsymbol{\nu}}\cdot\hat{\mathbf{y}})^2\right], \tag{24}$$

$$H_2^{-2(p)}(\nu;\hat{\mathbf{p}}_d) \equiv -2\sqrt{\frac{3}{5}}\frac{1}{[1+(\mathrm{NA}/n_o)^2]}A^{(p)}(\nu)(\hat{\boldsymbol{\nu}}\cdot\hat{\mathbf{x}})(\hat{\boldsymbol{\nu}}\cdot\hat{\mathbf{y}}), \tag{25}$$

and

$$A^{(p)}(\nu) \equiv \frac{2}{\pi}\left[\arccos\left(\frac{\nu}{2\nu_o}\right) - \frac{\nu}{2\nu_o}\sqrt{1-\left(\frac{\nu}{2\nu_o}\right)^2}\right]\Pi\left(\frac{\nu}{2\nu_o}\right), \tag{26}$$

$$B^{(p)}(\nu) \equiv \frac{1}{\pi}\left(\frac{\mathrm{NA}}{n_o}\right)^2\left[\arccos\left(\frac{\nu}{2\nu_o}\right) - \left[3-2\left(\frac{\nu}{2\nu_o}\right)^2\right]\frac{\nu}{2\nu_o}\sqrt{1-\left(\frac{\nu}{2\nu_o}\right)^2}\right]\Pi\left(\frac{\nu}{2\nu_o}\right), \tag{27}$$

$$C^{(p)}(\nu) \equiv \frac{1}{\pi}\left(\frac{\mathrm{NA}}{n_o}\right)^2\left[-\frac{4}{3}\frac{\nu}{2\nu_o}\sqrt[3]{1-\left(\frac{\nu}{2\nu_o}\right)^2}\right]\Pi\left(\frac{\nu}{2\nu_o}\right). \tag{28}$$

Figures 3 and 4 show plots of the spatio-angular OTF for two different polarizer orientations. Notice that the polarizer does not change the spatial band limit of the microscope, but it does change the contrast at high frequencies. If we use the cutoff frequency as a resolution criterion, we would conclude that polarizers do not change the spatial resolution of our microscope. However, if we use a spatial-domain resolution criteria like the Rayleigh or Sparrow criteria, then we would conclude that adding a polarizer improves the spatial resolution in the direction perpendicular to the polarizer.

Notice that the H_0^0 term in Figure 3 is negative for spatial frequencies near the cutoff frequency parallel to the polarizer transmission axis. This means that we expect to see a contrast inversion for angularly uniform distributions of dipoles when the spatial frequency pattern is parallel to the polarizer transmission axis. In

the spatial domain, this contrast inversion is caused by the elongation of the point spread function. The point spread function is wide enough that three fluorescent points spaced near the cutoff frequency give an intensity minimum that reports the position of the central fluorescent point—see Figure 5.

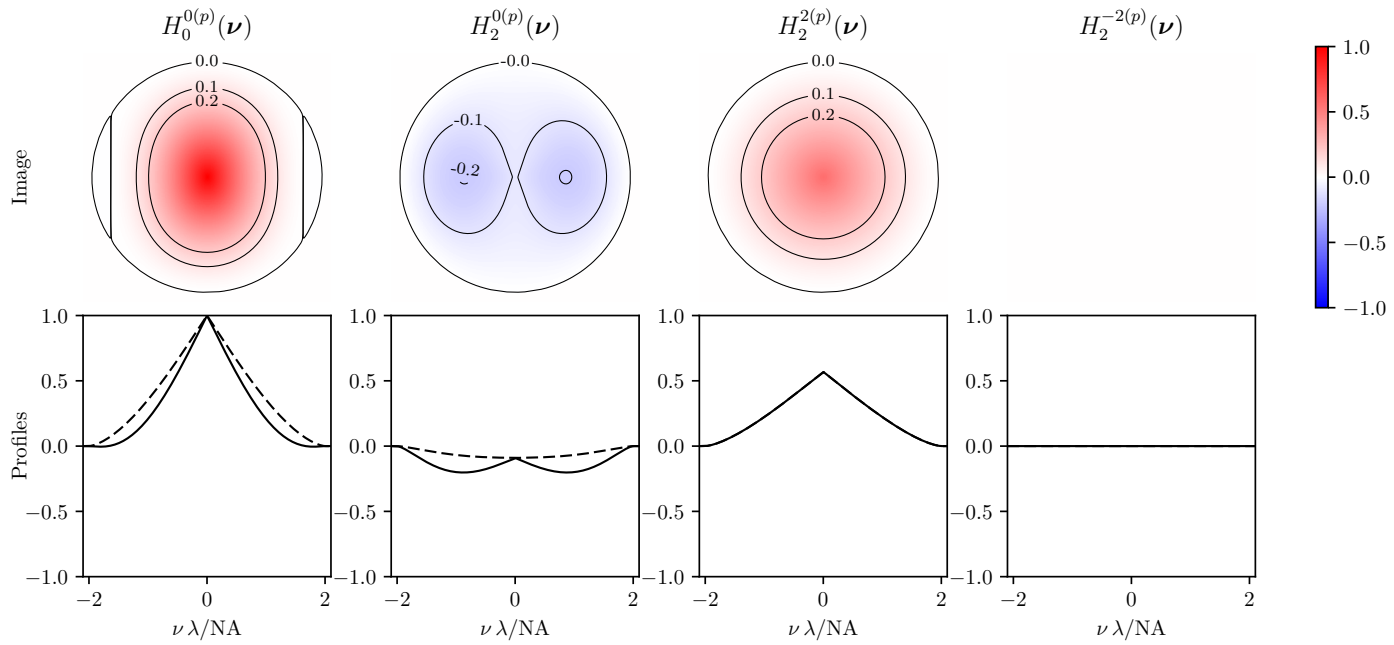

Figure 3: Spatio-angular orientation transfer function for a single-view fluorescence microscope with NA = 0.8, $n_o = 1.33$ and an $\hat{\mathbf{x}}$-oriented polarizer under the paraxial approximation. **Columns:** Each term of the spatio-angular optical transfer function. **Row 1:** Images of each term and **Row 2:** horizontal (solid) and vertical (dashed) profiles through each term.

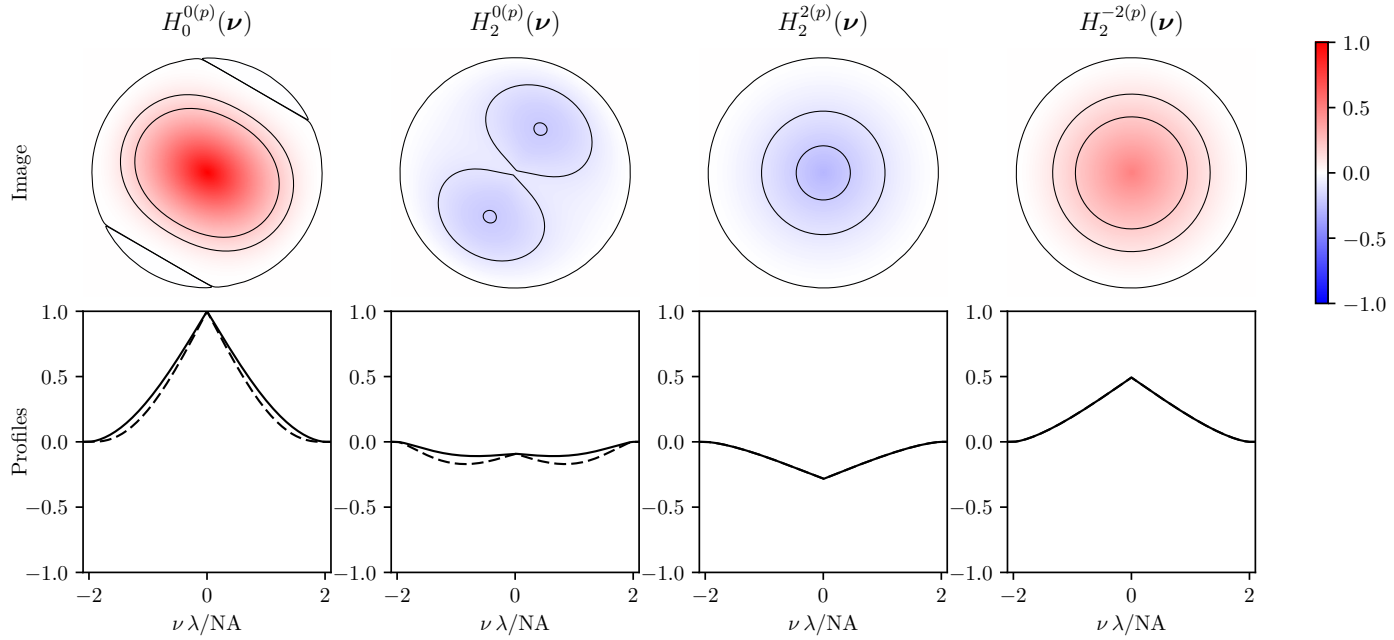

Figure 4: Spatio-angular orientation transfer function for a single-view fluorescence microscope with NA = 0.8, $n_o = 1.33$ and an $(\hat{\mathbf{x}}/2 + \sqrt{3}\hat{\mathbf{y}}/2)$-oriented polarizer under the paraxial approximation. **Columns:** Each term of the spatio-angular optical transfer function. **Row 1:** Images of each term and **Row 2:** horizontal (solid), and vertical (dashed) profiles through each term.

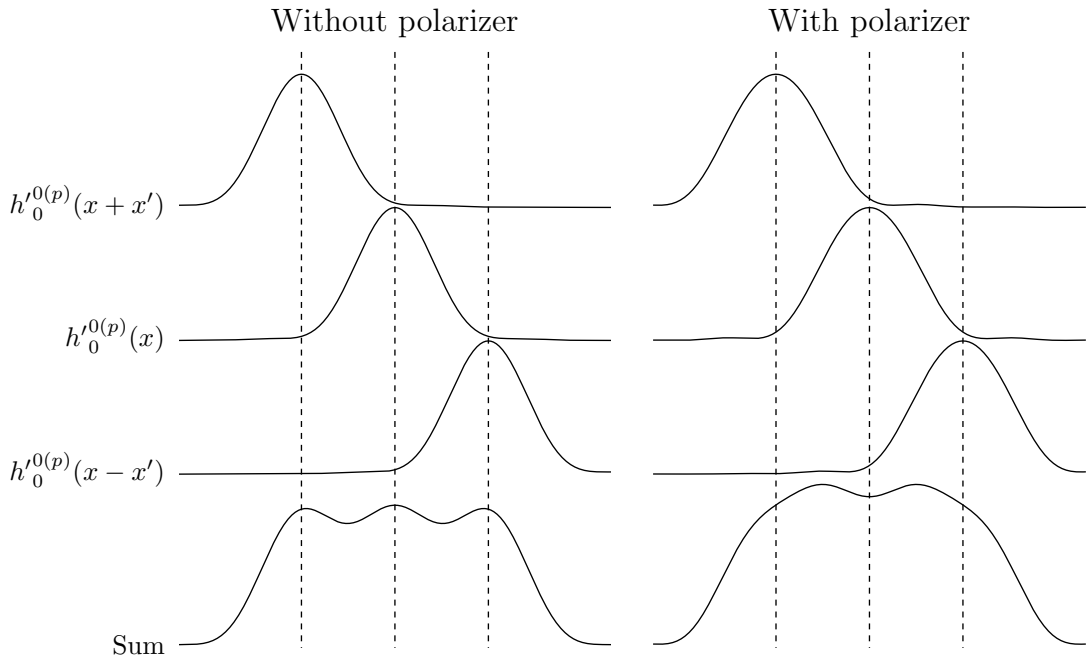

Figure 5: A polarizer creates a contrast inversion for uniformly distributed dipoles at high spatial frequencies along the direction parallel to the polarizer transmission axis. **Column 1:** Without a polarizer, three point sources with an angularly uniform distribution create an intensity pattern with three distinct peaks—the peaks report the position of the point sources. **Column 2:** With a polarizer, the point sources create an intensity pattern with two central peaks—the valley reports the position of the central point source. All of the sources in the figures are "resolvable" in the sense that they are spaced at a distance greater than the inverse of the cutoff frequency. This figure demonstrates contrast inversion at high spatial frequencies parallel to the polarizer transmission axis.

A Rotation of spherical harmonics

Given a spherical function and its spherical harmonic coefficients c_j (where j is a single index over the spherical harmonics), the spherical harmonic coefficients of the rotated function c'_i can be computed with the linear transformation

$$c'_i = \sum_j M_{ij} c_j, \tag{29}$$

where the elements of the linear transformation can be computed with

$$M_{ij} = \int_{\mathbb{S}^2} d\hat{\mathbf{s}}_o \, y_j(\mathbf{R}\hat{\mathbf{s}}_o) y_i(\hat{\mathbf{s}}_o), \tag{30}$$

where $\mathbf{R}$ is the rotation matrix that maps the original function to the rotated function [2]. If we assemble the elements of the linear transformation into a matrix $\mathbf{M}$, then the matrix is block sparse

$$\mathbf{M} = \left[\begin{array}{c|ccc|ccccc c} 1 & 0 & 0 & 0 & 0 & 0 & 0 & 0 & 0 & \cdots \\ \hline 0 & \mathbf{X} & \mathbf{X} & \mathbf{X} & 0 & 0 & 0 & 0 & 0 & \cdots \\ 0 & \mathbf{X} & \mathbf{X} & \mathbf{X} & 0 & 0 & 0 & 0 & 0 & \cdots \\ 0 & \mathbf{X} & \mathbf{X} & \mathbf{X} & 0 & 0 & 0 & 0 & 0 & \cdots \\ \hline 0 & 0 & 0 & 0 & \mathbf{X} & \mathbf{X} & \mathbf{X} & \mathbf{X} & \mathbf{X} & \cdots \\ 0 & 0 & 0 & 0 & \mathbf{X} & \mathbf{X} & \mathbf{X} & \mathbf{X} & \mathbf{X} & \cdots \\ 0 & 0 & 0 & 0 & \mathbf{X} & \mathbf{X} & \mathbf{X} & \mathbf{X} & \mathbf{X} & \cdots \\ 0 & 0 & 0 & 0 & \mathbf{X} & \mathbf{X} & \mathbf{X} & \mathbf{X} & \mathbf{X} & \cdots \\ 0 & 0 & 0 & 0 & \mathbf{X} & \mathbf{X} & \mathbf{X} & \mathbf{X} & \mathbf{X} & \cdots \\ \vdots & \vdots & \vdots & \vdots & \vdots & \vdots & \vdots & \vdots & \vdots & \ddots \end{array}\right]. \tag{31}$$

This means the spherical harmonic coefficients from each band transform independently from the other bands.

To efficiently find the point spread functions and transfer functions for the diSPIM we will compute the spherical harmonic coefficient transformation matrix for a rotation that maps the $\hat{\mathbf{z}}$ axis to the $\hat{\mathbf{x}}$. The rotation matrix is given by

$$\mathbf{R}_{\hat{\mathbf{z}}\to\hat{\mathbf{x}}} = \begin{bmatrix} 0 & 0 & 1 \\ 0 & 1 & 0 \\ -1 & 0 & 0 \end{bmatrix}, \tag{32}$$

and the spherical harmonic coefficient transformation matrix is given by

$$\mathbf{M}_{\hat{\mathbf{z}}\to\hat{\mathbf{x}}} = \left[\begin{array}{c|ccc|ccccc c} 1 & 0 & 0 & 0 & 0 & 0 & 0 & 0 & 0 & \cdots \\ \hline 0 & 0 & 0 & 1 & 0 & 0 & 0 & 0 & 0 & \cdots \\ 0 & 0 & 1 & 0 & 0 & 0 & 0 & 0 & 0 & \cdots \\ 0 & -1 & 0 & 0 & 0 & 0 & 0 & 0 & 0 & \cdots \\ \hline 0 & 0 & 0 & 0 & -1/2 & 0 & 0 & \sqrt{3}/2 & 0 & \cdots \\ 0 & 0 & 0 & 0 & 0 & -1 & 0 & 0 & 0 & \cdots \\ 0 & 0 & 0 & 0 & 0 & 0 & 0 & 0 & -1 & \cdots \\ 0 & 0 & 0 & 0 & \sqrt{3}/2 & 0 & 0 & 1/2 & 0 & \cdots \\ 0 & 0 & 0 & 0 & 0 & 0 & 1 & 0 & 0 & \cdots \\ \vdots & \vdots & \vdots & \vdots & \vdots & \vdots & \vdots & \vdots & \vdots & \ddots \end{array}\right], \tag{33}$$

when the matrix elements are ordered as $[y_0^0|y_1^1, y_1^{-1}, y_1^0|y_2^0, y_2^1, y_2^{-1}, y_2^2, y_2^{-2}]$. For more complicated transformations (higher order coefficients or arbitrary rotations) we can use recurrence relations to find the spherical harmonic coefficient transformation matrix [3].

References

[1] Talon Chandler, Shalin Mehta, Hari Shroff, Rudolf Oldenbourg, and Patrick J. La Rivière. Single-fluorophore orientation determination with multiview polarized illumination: modeling and microscope design. *Opt. Express*, 25(25):31309–31325, Dec 2017.

[2] Jan Kautz, Peter-Pike Sloan, and John Snyder. Fast, arbitrary BRDF shading for low-frequency lighting using spherical harmonics. In *Proceedings of the 13th Eurographics Workshop on Rendering*, EGRW '02, pages 291–296, Aire-la-Ville, Switzerland, Switzerland, 2002. Eurographics Association.

[3] Joseph Ivanic and Klaus Ruedenberg. Rotation matrices for real spherical harmonics. direct determination by recursion. *The Journal of Physical Chemistry*, 100(15):6342–6347, 1996.